Journal of Structural Geology 91 (2016) 88–101

Contents lists available at ScienceDirect

Journal of Structural Geology

journal homepage: www.elsevier.com/locate/jsg

Strain partitioning into dry and wet zones and the formation of Ca-rich myrmekite in syntectonic syenites: A case for melt-assisted dissolution-replacement creep under granulite facies conditions

G.B. De Toni [a, *], M.F. Bitencourt [a, b], L.V.S. Nardi [a, b]

[a] Programa de Pós-graduação em Geociências, Instituto de Geociências, Universidade Federal do Rio Grande do Sul, Av. Bento Gonçalves, 9500, Porto Alegre, 91500-000, RS, Brazil
[b] Departamento de Geologia, Instituto de Geociências, Universidade Federal do Rio Grande do Sul, Av. Bento Gonçalves, 9500, Porto Alegre, 91500-000, RS, Brazil

ARTICLE INFO

Article history:
Received 11 January 2016
Received in revised form
26 July 2016
Accepted 7 August 2016
Available online 11 August 2016

Keywords:
Syntectonic magmatism
Syntectonic syenites
Myrmekite
Dissolution-replacement creep
Strain partitioning
Granulite facies conditions

ABSTRACT

The formation of Ca-rich myrmekites is described in syntectonic syenites crystallized and progressively deformed under granulite facies conditions. The syenites are found in high- and low-strain zones where microstructure and mineral composition are compared. Heterogeneously distributed water-rich, late-magmatic liquids were responsible for strain partitioning into dry and wet high-strain zones at outcrop scale, where contrasting deformation mechanisms are reported. In dry high-strain zones K-feldspar and clinopyroxene are recrystallized under high-T conditions. In wet high-strain zones, the de-stabilization of clinopyroxene and pervasive replacement of relatively undeformed K-feldspar porphyroclasts by myrmekite and subordinate micrographic intergrowths indicate dissolution-replacement creep as the main deformation mechanism. The reworking of these intergrowths is observed and is considered to contribute significantly to the development of the mylonitic foliation and banding. A model is proposed for strain partitioning relating a positive feedback between myrmekite-forming reaction, continuous inflow of late-magmatic liquids and dissolution-replacement creep in the wet zone at the expenses of original mineralogy preserved in the dry zones. Melt-assisted dissolution-replacement creep in syntectonic environments under granulite-facies conditions may extend the field of operation of dissolution-replacement creep, changing significantly the rheology of the lower continental crust.

1. Introduction

Myrmekite is one of the most commonly described and discussed microscopic feature in geology. This is partly due to its common ocurrence in a diversity of rocks and environments, and also because of the controversy generated since the early debate between the two proposed models for its genesis by replacement (Becke, 1908) and exsolution (Schwantke, 1909). With the advances in both science and technology, mainly with the advent of the scanning-electron microscope and microprobe, detailed observations of composition and morphology of minerals and microstructures have lead to great advances in the understanding of replacement reactions. Years of research on the subject have produced extensive literature (see Phillips, 1974 for a review of early concepts), and a strong tendency is observed toward a balance of arguments from both schools of thought (Ashworth, 1972; Phillips, 1980). In a compromising paper, Phillips (1980) suggests that the exsolution model is best applied to undeformed granitoids, whilst the replacement model generally fits better to deformed and metamorphosed rocks. He also argued that both models could operate together (as agreed upon by Ashworth, 1972; Tsurumi et al., 2003).

Myrmekite is strictly defined as a symplectitic intergrowth of sodic plagioclase (generally oligoclase) and vermicular quartz in contact or pseudomorphically replacing K-feldspar (Phillips, 1974; Smith and Brown, 1988; Vernon, 2004). Calcic myrmekites are reported (e.g. Dymek and Schiffries, 1987; Efimov et al., 2010; Mukai et al., 2014) as resulting from the replacement of intermediate-An content plagioclase by more calcic ones in mafic rocks. However, some authors (as Smith and Brown, 1988) suggest that such

* Corresponding author.
E-mail address: gdetoni@ufrgs.br (G.B. De Toni).

http://dx.doi.org/10.1016/j.jsg.2016.08.002
0191-8141/

intergrowth should not be taken under the term myrmekite, but simply referred to as symplectites of quartz and plagioclase. In this paper we consider myrmekite as a symplectite formed by vermicular quartz hosted in plagioclase (independent of its An content) in contact or pseudomorphically replacing an adjacent feldspar. As previous publications attribute to the myrmekitic plagioclase a more calcic composition than its host, myrmekite genesis may be conceived as a feldspar calcification reaction.

The correlation between deformation and myrmekite genesis was well demonstrated in amphibolite-facies mylonitic granites by Simpson and Wintsch (1989) as the result of incongruent pressure solution at the compressive quadrants of asymmetric K-feldspar porphyroclasts. The close relationship between myrmekite and deformation is supported by many other papers since then, as Vernon (1991), Tsurumi et al. (2003) and Menegon et al. (2006, 2008).

On the other hand, the importance of fluids is illustrated by Abart et al. (2014) who describe myrmekite formation on perthitic orthoclase megacrysts of the undeformed, pyroxene-bearing variety of the Weinsberg Granite (South Bohemian Batolith, Austria). In these rocks, myrmekite genesis is interpreted to be synchronous with and related to orthopyroxene hydration and replacement of plagioclase by biotite at around 500 °C. The authors attribute such reactions to late-stage, post-magmatic, hydrothermal transformations, and consider that the system was closed at the sample-scale but open (metasomatic) at the crystal-scale.

Some key questions concerning the relative importance of deformation and fluids in the genesis of myrmekite in deformed rocks were addressed by Vernon (1991) and remain under discussion. This author describes myrmekite overgrowing non-deformed K-feldspar and simultaneously recrystallized at the rear of the growing lobes, which means that syn-deformational myrmekite is metastable. Based on this evidence he suggests, as opposed to Simpson and Wintsch (1989), that strain energy is not the major contributing factor for myrmekite nucleation and growth, but may contribute indirectly by facilitating the access of fluids to growth sites. This is supported by a volume loss resulting from the myrmekite forming-reaction, which in turn facilitates the access of fluids and promotes the continuity of the reaction. This negative volume change was calculated by Simpson and Wintsch (1989) at approximately 10%, and is also supported by calculations of 8.5% volume loss by Menegon et al. (2006).

The role of fluids and deformation in myrmekite genesis was more recently addressed by Menegon et al. (2006) who showed that both factors may compete for the main control of myrmekite-forming reactions. Their study of lower-amphibolite facies metagranites in the Gran Paradiso nappe (North-western Alps) has demonstrated that at initial stages of deformation, stress and elastic strain concentrations at perthite lamellae and microcline twinning are the triggering factors to start the reaction. However, fluids appear to become increasingly important as deformation proceeds and cause widespread myrmekite formation, which in turn leads to reaction-softening. The same authors (2006, 2008) interpret these myrmekites as products of dissolution-precipitation creep. A similar case is reported by Wintsch and Yi (2002) who consider dissolution and replacement creep as fluid-dependent deformation mechanisms that may operate in wet rocks even at relatively high temperatures (mid crustal levels/amphibolite facies conditions). Dislocation creep would then be restricted to the high temperatures and dry conditions of the lower crust. Despite the generally dry, or H_2O-poor conditions of the lower continental crust, significant amounts of melt may be present, as pointed out by Etheridge et al. (1983). Melt-assisted dissolution and re-precipitation could be effective at granulite facies conditions, as described by Álvares-Valero et al. (2005) in metapelitic residual enclaves from the Neogene Volcanic Province (SE Spain).

In this paper we focus on the microstructures of a Neoproterozoic syntectonic syenite in southernmost Brazil which was crystallized and progressively deformed under granulite facies conditions. In high-strain zones, mylonitic syenites of variable microstructure and mineral compositions are interleaved and heterogeneously injected by later leucocratic veins. Pervasive myrmekites are restricted to the bands containing several injections, which is suggestive of fluid-related strain partitioning and the operation of different deformation mechanisms.

2. Samples and methods

The results of an integrated approach of fieldwork, petrography, SEM and microprobe analysis are presented in this paper. A representative outcrop from a high-strain zone of the Arroio das Palmas Syenite was selected for detailed observations and sampling (UTM coordinates: 338533 mE/6637552 mN; Fuse 22J, Córrego Alegre datum). Two representative samples of highly-deformed varieties (02B and 02G) were chosen from this key-outcrop. They are compared in terms of mineral composition and microstructure with an undeformed one (sample 07B; UTM coord. 337034 mE/6641995 mN) taken from a low-strain zone. The results obtained independently by different techniques will be presented integrated in subsections for each studied sample.

Modal compositions were obtained by thin-section point-counting using Hardledge® software (www.endeeper.com). Modal analyses performed on undeformed (07B) and highly-deformed (02B) samples resulted in about 560 points from each thin-section. In another highly-deformed sample (02G), a total of 1449 points were counted from two adjacent thin sections. Other 147 points were obtained from a 0.1 mm-wide, fine-grained band of the same sample.

SEM analyses were carried out at the Isotope Geology Laboratory of Universidade Federal do Rio Grande do Sul (Brazil), using a JEOL JSM-6610LV microscope, with carbon coat and 15 keV current. Microprobe analyses were performed at the Microprobe Laboratory of the same University, using a Cameca SXFive. The analytical conditions were 14.8 keV, 15 nA current, and beam size of 20 μm.

3. Geological setting

3.1. Geotectonic framework

The study area is located in the central-northern portion of the Sul-rio-grandense Shield (SRGS - Fig. 1a). The SRGS, together with the shield areas in Santa Catarina and Uruguay form the southern segment of the Mantiqueira Province, which is a Neoproterozoic orogenic feature resulting from the amalgamation of Gondwana (Almeida et al., 2000). Cratonic inliers of Paleoproterozoic to Archaean ages occur in the southwestern part of the SRGS, but the so-called Rio de La Plata Craton is best exposed in the Uruguayan Shield. The Neoproterozoic record in the SRGS is present in the Dom Feliciano Belt, which is described and subdivided in terms of three major domains (Fernandes et al., 1992). The juvenile rock association adjacent to the cratonic area (Fig. 1a) is interpreted as a former continental magmatic arc of 753–680 Ma (Hartmann et al., 2011). In the central portion of the SRGS, low-to medium-grade supracrustal metamorphic rocks are partly covered by a Neoproterozoic to Cambrian volcano-sedimentary succession. The eastern part features a large volume of post-collisional granites called Pelotas Batolith (Philipp and Machado, 2005). The granites are structurally controlled by the Southern Brazilian Shear Belt (SBSB – Bitencourt and Nardi, 2000), which is an anastomosed

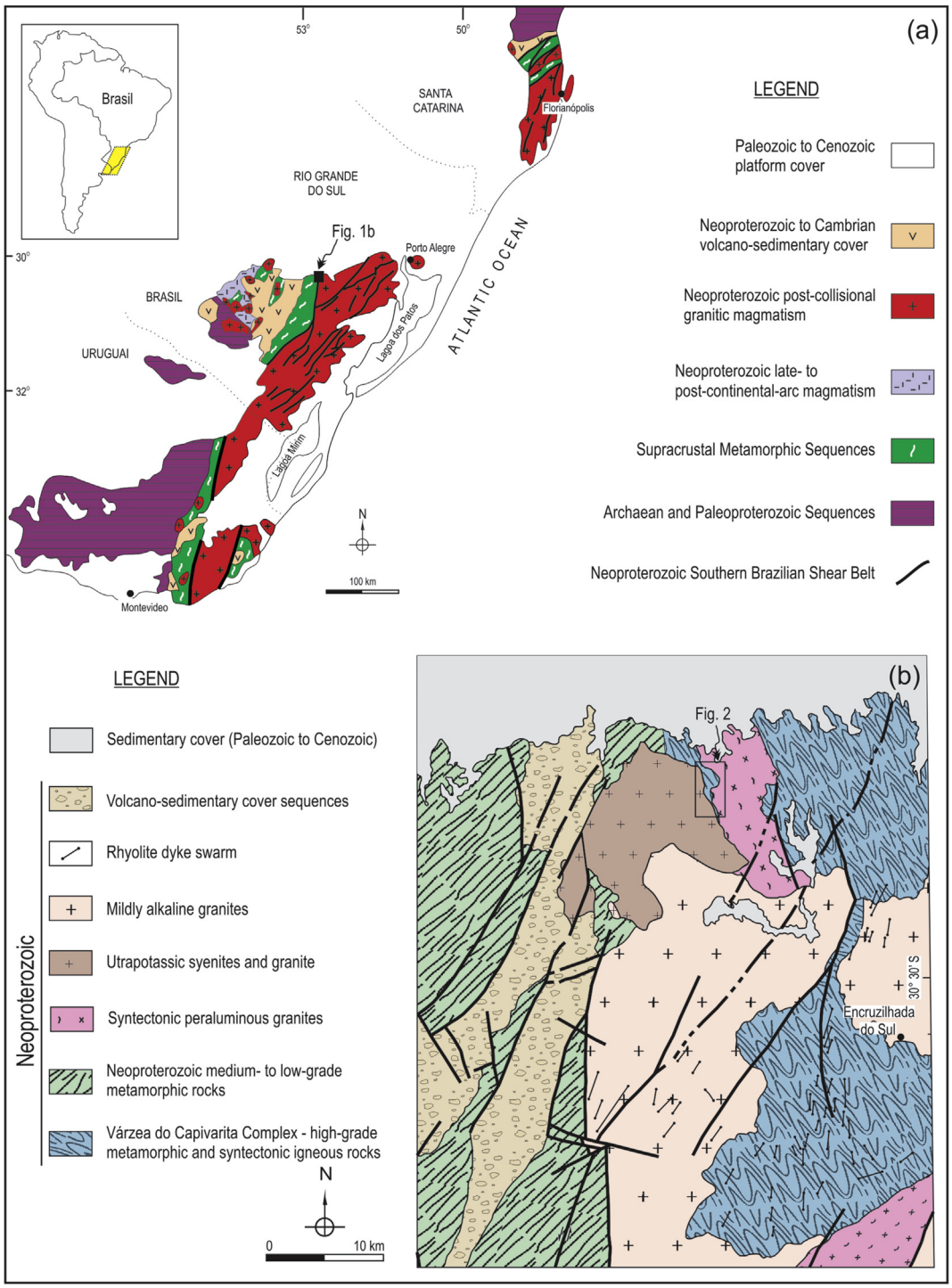

Fig. 1. (a) Geotectonic domains in the southern segment of the Mantiqueira Province, from southern Brazil to Uruguay (modified from Bitencourt and Nardi, 2000). (b) Regional geological map with location of the study area (modified from Martil et al., 2011).

translithospheric framework of shear zones that has acted as conduit for magmas through the crust and also promoted decompression of shallower levels of the mantle during late-Neoproterozoic times. The rocks reported in this paper are located at the northwestern border of the Pelotas Batholith (Fig. 1b), where a NNW-trending branch of the SBSB has conditioned the intrusion of syntectonic peraluminous granites (Niessing et al., 2011) and ultrapotassic syenites (object of this paper; Bitencourt et al., 2013). The NNW-trending structures comprise gently-dipping and steeply-dipping shear zones formed by progressive deformation under granulite facies conditions. They are present in the syenites as well as in the metamorphic wall rocks.

3.2. Local geology

The Várzea do Capivarita Complex (VCC) comprises granulite facies gneisses and syntectonic intrusive syenites. It is part of the roof of the Pelotas Batholith post-collisional granites and forms patches of several square kilometers near its northwestern limit (Fig. 1b). Pelitic and calcsilicate paragneisses are the dominant rocks in the VCC, whilst orthogneisses form a subordinate volume.

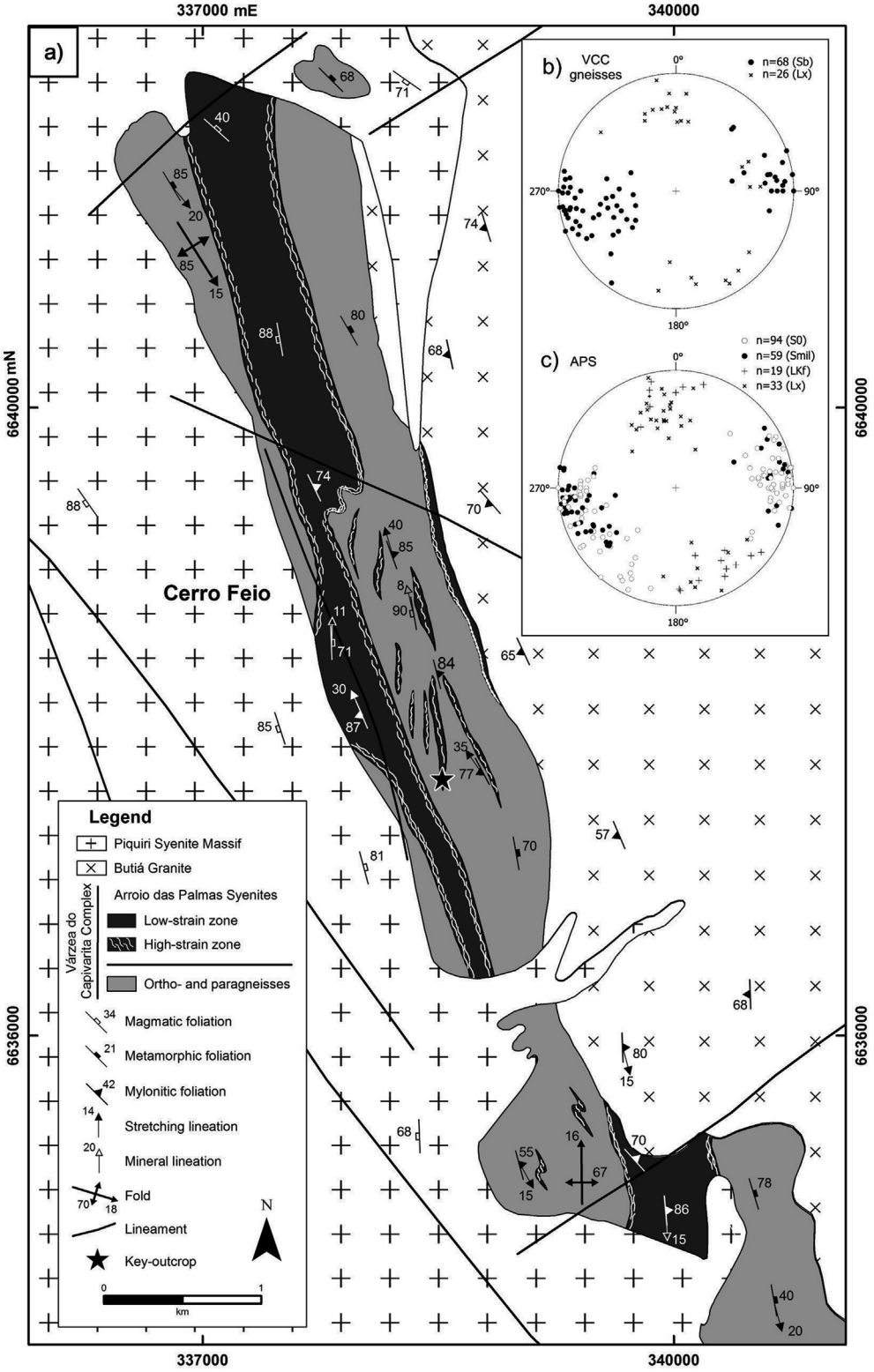

Fig. 2. Geological features of the Arroio das Palmas Syenite and host rocks. (a) Geological map, with indication of detailed outcrop. (b-c) Lower-hemisphere, equal-area projections of structural elements from APS and host rocks.

Interleaving of different lithological types at multiple scales is due to shearing of a thrust pile under granulite facies conditions, as described by Martil et al. (submitted to publication). The geometry of this thrust pile is only locally preserved. Progressive deformation in a transpressive regime has lead to dextral shearing along sub-vertical zones that follow the same NNW regional trend (Fig. 2a) and contain sub-horizontal stretching lineations (Fig. 2b). The granulite facies conditions of metamorphism in the VCC are referred by Philipp et al. (2015) as 720–820 °C and 8–9 kbar. Peak metamorphism was dated at 648 ± 5 Ma (U-Pb SHRIMP in zircon – Martil et al., subm.), interpreted as the approximate age of collision. Similar metamorphic age values are reported for this complex by Chemale Jr. et al. (2011) as 651 ± 9 Ma (LA-ICP-MS, U-Pb in titanite).

The Arroio das Palmas Syenite (APS) is the intrusive part of the VCC in the study area and will be described in detail next. The Butiá Granite (eastern part of Fig. 2a) is a syntectonic, sillimanite-bearing peraluminous granite emplaced along a NNW-striking transcurrent shear zone that is part of the Southern Brazilian Shear Belt. Magmatic ages obtained in monazite point to a crystallization age of 629 ± 7 Ma (U-Pb ID-TIMS, Bitencourt et al., 2015). The Piquiri Syenite Massif (western part of Fig. 2a) is a late-tectonic intrusion of *ca.* 611 Ma (Philipp et al., 2002).

3.3. The Arroio das Palmas Syenite

The syntectonic character of the APS is indicated by several features, such as (i) the magmatic foliation of the syenite is parallel to a mylonitic foliation conformable to intrusion contacts; (ii) both structures are parallel to the metamorphic banding of the wallrocks formed under granulite facies conditions (Fig. 2b-c); (iii) microstructures of the deformed syenite varieties developed under high-temperature conditions, as discussed in this paper; (iv) the magmatic age obtained in a virtually undeformed variety of the syenites (642 ± 10 Ma, LA-ICP-MS zircon – Bitencourt et al., 2011), is situated within error of the 648 ± 5 value reported by Martil et al. (submitted) for the granulite facies metamorphism. Concordant to subconcordant intrusive relations are best seen in low-strain zones, where intrusion geometry is preserved from further deformation (Fig. 3a).

The APS main rock type is a porphyritic syenite containing *ca.* 40% of megacrystic, white K-feldspar (Kfs - *ca.* 2 cm) set in a mafic-rich, medium-grained groundmass composed of biotite and clinopyroxene (Cpx) with minor amounts of amphibole and interstitial quartz. Zircon and apatite are the main accessory phases. A subordinate variety is a medium-to fine-grained, inequigranular syenite of similar composition. Scattered, subhedral Kfs megacrysts are commonly found in the finer-grained syenite (Fig. 3b), and cm-long lenses of the fine-grained variety in the porphyritic one (upper part of Fig. 3b) are interpreted as indicative of their co-magmatic character. Fine-to medium-grained leucosyenites or syenogranites are found as predominantly concordant, but occasionally discordant, cm-thick veins crosscutting the other varieties (Fig. 3b). They are interpreted to represent the late-stages of the APS magmatism.

The APS forms several foliated (Fig. 3c), concordant tabular bodies of variable thickness (centimeters to tens of meters) intrusive in the metamorphic rocks. Their internal structure is given by the cm-to m-alternation of the two main varieties (Fig. 3b), and a similar relation is observed between the APS and the VCC gneisses.

The APS textural variation is enhanced by the heterogeneous development of solid-state deformation under high-temperature conditions (Fig. 3b-d). The progressive character of the subsolidus deformation relative to the magmatic structures of the APS is defined as a gradual transition from high-to low-strain zones which alternate at variable scales, from hundreds of meters (Fig. 2a) to

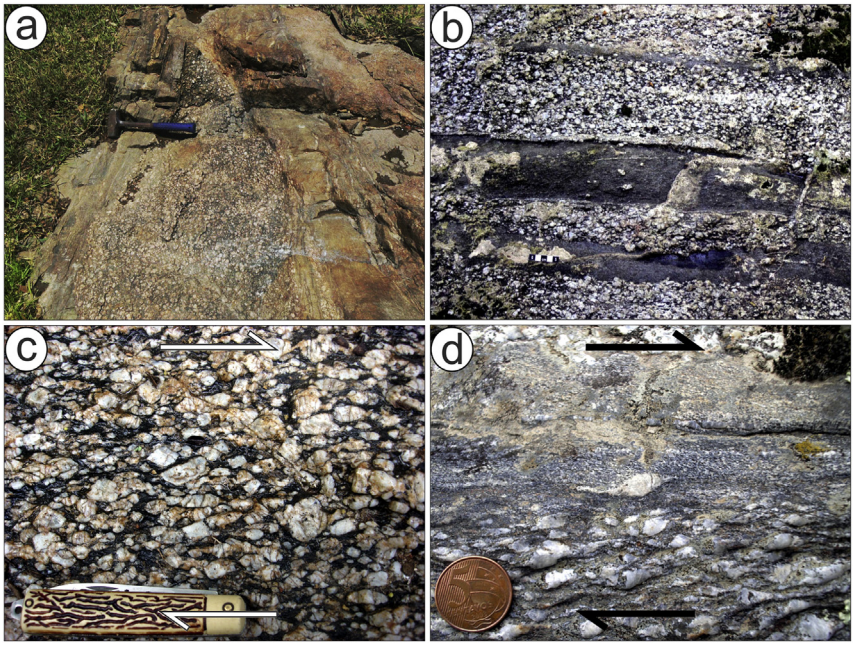

Fig. 3. Mesoscale features of the APS. (a) Intrusive contact of APS porphyritic variety in paragneisses of the VCC as preserved within a low-strain zone. Notice the greater thickness of the injection in the foreground and the thinner tip in perspective, which suggests opening of the wall rock foliation. (b) Fine-grained varieties alternating with porphyritic ones either as tabular bodies of sharp contacts (center and lower part) or as highly-elongate lenses of diffuse contacts (upper part). Irregular contacts and variable amount of scattered Kfs megacrysts within the fine-grained rocks indicate their coeval character. Leucocratic, cm-thick injections are either parallel or oblique to the main foliation. (c) Weakly-deformed porphyritic syenite observed on XZ plane. Most of the aligned subhedral Kfs megacrysts mark the foliation trace (parallel to the photograph base) and some oriented anticlockwise oblique crystals indicate dextral shear sense. (d) Highly-deformed porphyritic (lower part) and fine-grained (upper part) syenites observed on XZ plane. At the contact (center of the photograph), the long recrystallization tails of a strongly deformed, asymmetric porphyroclast indicate dextral shear-sense.

outcrop scale. Low-strain zones are recognized for the preservation of igneous textures whilst in high-strain zones recovery and recrystallization features are widespread.

4. Structural features and mineral composition of the APS in low-strain zones

The APS has a generally well-developed, steeply-dipping igneous foliation marked by the shape alignment of Kfs megacrysts and biotite flakes, and by elongate aggregates of equant clinopyroxene. The shape alignment of Kfs also defines a shallow to medium-plunge mineral lineation. When observed in the plane perpendicular to the foliation and parallel to the lineation (XZ plane) some Kfs megacrysts are oriented anticlockwise oblique to the foliation trace indicating dextral shear sense (Fig. 3c).

The main textural feature of the APS undeformed rocks is given by aligned Kfs megacrysts surrounded by mafic groundsmass (Fig. 4a). Kfs composition ranges from $Or_{87}Ab_{13}$ to $Or_{97}Ab_{03}$ (Fig. 5a), and the crystals commonly have fine perthite lamellae (less than 0.1 mm thick). Wherever two Kfs megacrysts touch, swapped rim-type microstructures develop, either as perthite (Voll, 1960) or as fine (less than 0.1 mm) myrmekite (Vernon, 2004), as observed in the inset of Fig. 4a. In this case, plagioclase composition lies between $Ab_{77}An_{22}$ and $Ab_{89}An_{10}$ with optical orientation

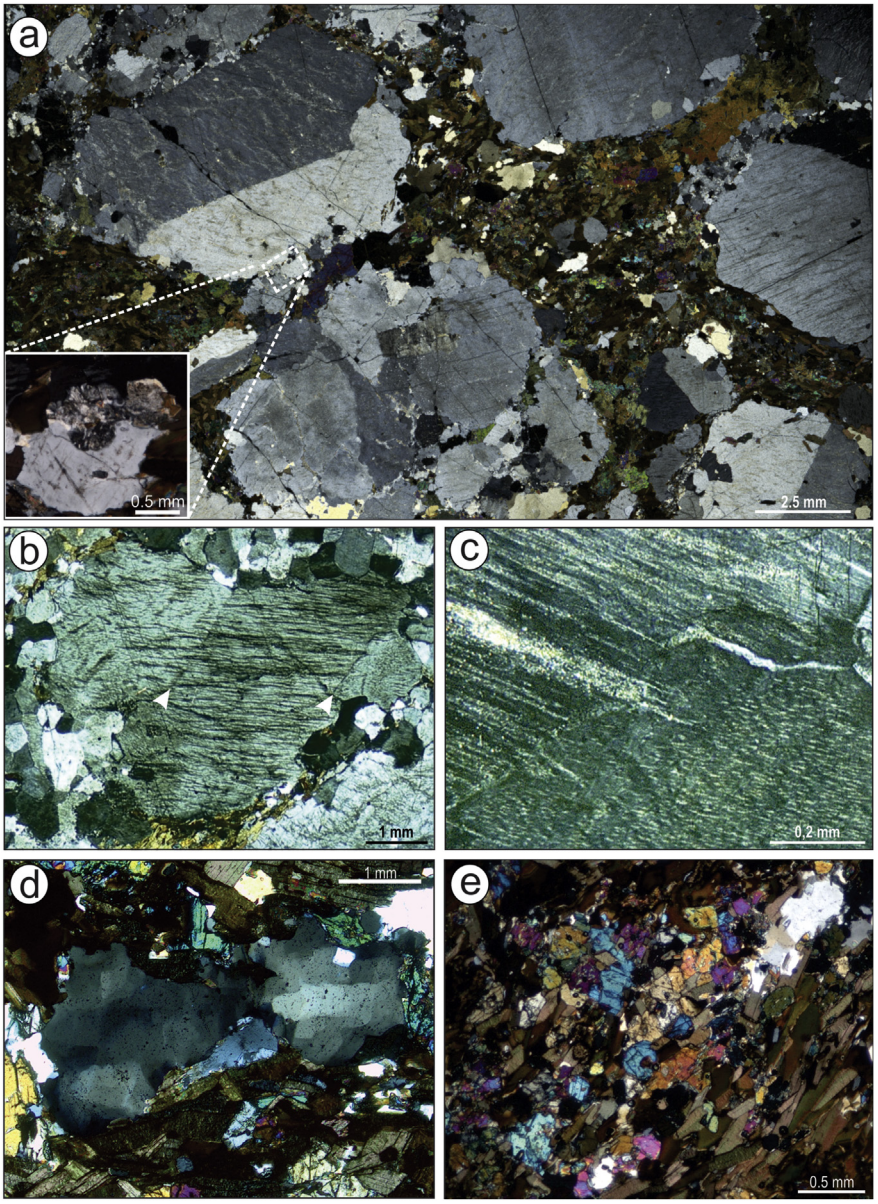

Fig. 4. Microstructural features of the undeformed APS. (a) Thin-section scan showing the general aspect of least deformed porphyritic variety with subhedral, aligned Kfs megacrysts in mafic-rich groundmass; notice finer grains developed by exsolution and/or recrystallization where megacrysts touch. Inset highlights swapped rim myrmekites between two K-feldspars; (b) Perthitic K-feldspar megacryst locally surrounded by granoblastic feldspar grains which develop at the contact with another megacryst (upper right and left), and are absent where megacryst is in contact with the groudmass (bottom). Misorientation within the megacryst (white arrows) may be due either to subgrain boundaries or microcracks. The boundary at the top right is enlarged in (c) to show that perthite not only crosscuts them but also fills up the discontinuity. (d) Intersticial quartz with chessboard pattern subgrains; the surrounding groundmass is predominantly composed by biotite and cpx. (e) Detail of mafic groundmass texture, with aligned biotite flakes and cpx aggregates.

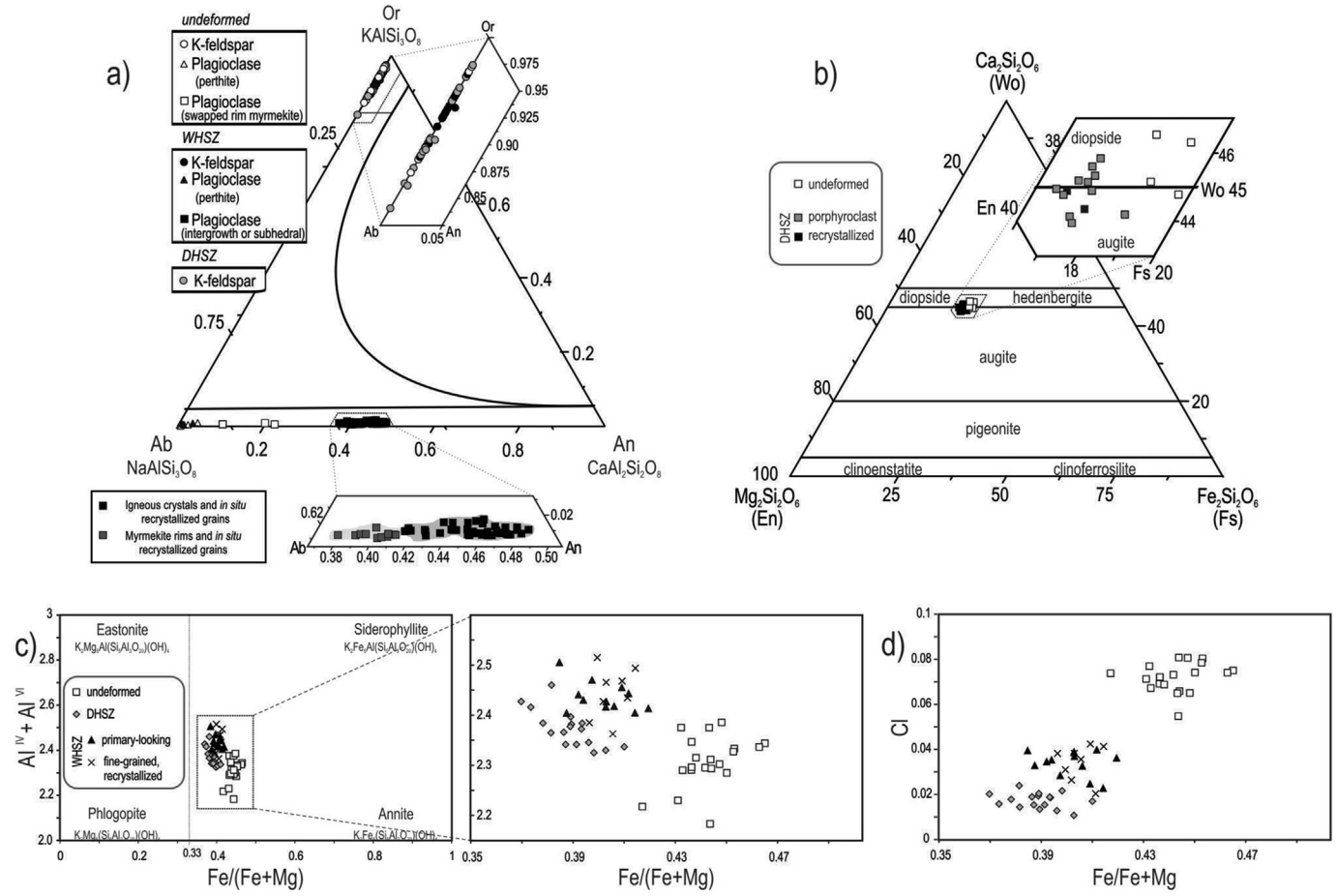

Fig. 5. APS mineral chemical compositions plotted on classification diagrams. Dashed lines indicate enlargement of the marked field. (a) Feldspar classification ternary diagram (solvus for low-P from Parsons and Brown, 1983) with the analysis of undeformed, DHSZ and WHSZ. Different symbols indicate different minerals, whilst different colours indicate different samples. (b) Cpx classification ternary diagram (Morimoto, 1988) with analyses of undeformed and DHSZ samples. (c) Biotite classification diagram (Deer et al., 1992). (d) Cl *vs*. Fe/(Fe + Mg) diagram where two different populations of biotite are discriminated mainly with respect to Cl a.f.u. content.

usually continuous with that of the neighbouring perthite, suggesting a common exsolution genesis for these microstructures.

In mesoscopically undeformed samples, microscopic evidence of intracrystalline deformation is recorded in Kfs megacrysts. Microcracks parallel to cleavages, undulose extinction and subgrains of 0.5–1 mm in diameter are locally observed (as in the center of Fig. 4a). Marginal recrystallization, with *ca.* 0.5 mm granoblastic grains, is mostly restricted to the border regions of interactive Kfs megacrysts (upper-right of Fig. 4a and b). Deformational features in these mesoscopically undeformed grains, like microcracks and/or subgrain boundaries, are locally cut or partly filled by perthite lamellae (Fig. 4c), which indicates that deformation was effective above the solvus temperature. Interstitial quartz usually exhibits chessboard pattern subgrains (Fig. 4d), indicative of high-T deformation (Mainprice et al., 1986; Kruhl, 1996). The main texture in the groundmass is defined by the orientation of biotite lamellae or clinopyroxene grains and aggregates which surround the megacrystic Kfs (Fig 4e).

The average Cpx composition is Wo_{45} $En_{34.7}$ $Fs_{18.7}$ $Aeg_{01.5}$ (Fig. 5b) overlapping the augite to diopside fields in the classification of Morimoto (1988). The grains are elongate to equant with maximum 0.5 mm size. They form elongate aggregates of up to 1 cm length, with subordinate amount of biotite.

Biotite forms *ca.* 1 mm long, well-aligned, reddish brown lamellae containing 0.05–0.1 mm apatite and zircon inclusions. The composition of biotite is characterized by low Fe/(Fe + Mg) ratios (0.417–0.463), $Al^t = (Al^{iv} + Al^{vi})$ between 2.18 and 2.38 (Fig. 5c), and high Ti and Cl content, ranging from 0.245 to 0.46 a.f.u., and from 0.54 to 0.80 a.f.u., respectively (Fig. 5d).

5. Structural features and mineral composition of APS in high-strain zones

5.1. Mesoscale features of high-strain zones

In high-strain zones (Fig. 6a) the foliation becomes even more well-developed as a result of progressive rotation of the Kfs porphyroclasts into alignment, and of their subsequent stretching into asymmetric, dextral shear sense recrystallization tails (Fig. 3d). A set of EW-striking, later subvertical antithetic shear bands is locally developed and drag the foliation with sinistral shear sense (upper right and lower left in Fig. 6a).

The presence of heterogeneously distributed leucogranite veins of variable thickness is remarkable, and their larger volumes coincide with the presence of dark-coloured, concordant, mm-to dm-thick bands of fine-grained, ultramylonitic rocks whose composition oscillates between that of a syenite and that of a (quartz + plagioclase)-rich rock (Fig. 6a). These veins are successively injected into the host syenites with the earlier ones being more strongly deformed along the main foliation, and locally

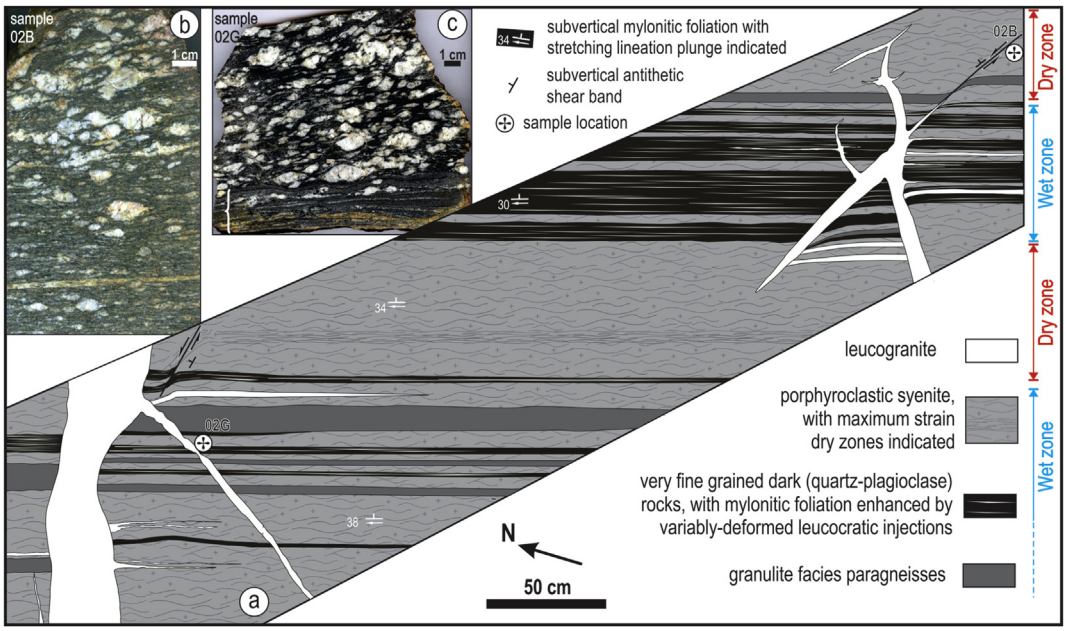

Fig. 6. (a) Outcrop sketch with main structural features, sample locations and rock slab photographs. (b) Sample 02B – dry high-strain zone. (c) Sample 02G – wet high-strain zone. The bracket highlights the band of (quartz-plagioclase) mylonitic rock in sharp contact with the porphyroclastic syenite which corresponds to the lower part of Fig. 9.

crosscut and displaced by younger and less deformed ones. The same vein commonly branches out to follow both the main foliation and antithetic shear bands (Fig. 6a, upper right corner), which again suggests the coeval character of these structures.

The correlation of the presence of nearby veins with the ocurrence of distinct mineral compositions in the mylonitic syenites (as described next) has led us to divide the studied outcrop in dry and wet high-strain zones (DHSZ – Fig. 6b, and WHSZ – Fig. 6c, respectively), which alternate at meter-scale. In the so-called dry zone leucogranite veins are virtually absent, whilst the wet zone is characterized by their concentration as a network that percolates and interacts with APS varieties and possibly has aided or triggered mineral changes.

In consequence, the DHSZ has a relatively homogeneous aspect when compared to the WHSZ. Within the DHSZ a gradual transition is observed between porphyroclast-rich and porphyroclast-poor bands, leading to cm-thick bands of highly-deformed, finer-grained syenites where the APS original composition is preserved (Fig. 6a and b). In contrast, porphyroclastic syenites from WHSZ are in sharp contact with the ultramylonitic varieties which may contain scattered, very elongate, residual porphyroclasts. The fine-grained rocks form cm-to dm-wide bands (indicated by bracket in Fig. 6c) or elongate, mm-wide lenses, and eventually become part of the recrystallized matrix and enhance the banded aspect of the resulting rock.

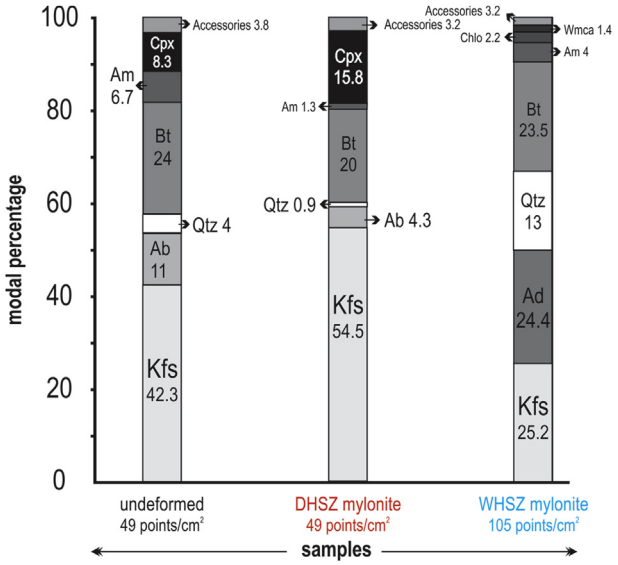

Fig. 7. Modal compositions for undeformed syenite, dry and wet high-strain zone mylonites. Mineral abbreviations from Kretz (1983) except Ad = andesine.

5.2. Compositional and microstructural variation across DHSZ and WHSZ

5.2.1. Comparative modal composition

In order to compare modal compositions of the studied samples, a bar graph is presented (Fig. 7) where it becomes clear that the dry zone mineralogical composition is equivalent to that of the undeformed syenite. In both samples the main mineral is Kfs (54.5 and 42.3%, respectively), the difference being due to the volume of exsolved albite (4.3 and 11%, respectively). The main mafic phases are biotite (20 and 24%) and clinopyroxene (15.8 and 8.3%), and quartz is subordinate (4 and 0.9%). In contrast, amphibole has some importance in the undeformed sample (6.7%) but is not significant in the deformed dry one (1.3%).

Although the undeformed sample is apparently more differentiated when compared with the DHSZ sample, as indicated by the proportion of quartz and relative proportion of amphibole to Cpx, it is sufficiently similar for the purpose of this comparison, and could be taken as an approximation of the protolith composition.

The mineralogical composition contrast of the wet zone sample relative to undeformed and dry zone samples is also clear, in that the wet zone sample shows amounts of Kfs and plagioclase of the same order (25.2 and 24.4%, respectively), and 13% of quartz. Biotite is still the main mafic phase (23.5%), but clinopyroxene disappears. Instead, a small amount of amphibole (4%) is found, together with

other secondary phases (chlorite, white mica, albite, sulphide and calcite).

A very fine grained, plagioclase-rich, quartz-feldspathic granoblastic groundmass (16.3%) surrounds Kfs porphyroclasts and sometimes forms elongate lenses interspersed with the mafic phases. The composition of the fine-grained matrix was quantified separately in one band (Ad 40.1, Qtz 27.9, Bt 17.7, Kfs 10.2 and Am 2%), and was computed together in the global composition of the WHSZ porphyroclastic syenite, as shown in Fig. 7.

On the other hand, the sum of hydrated phases of the WHSZ sample (31.1%) is similar to the sum of hydrated phases exhibited by the undeformed sample (30.7%), which is almost one and a half times greater than the sum of hydrated phases of the DHSZ sample (21.3%).

5.2.2. Microstructures and mineral composition of DHSZ

The typical DHSZ rock is a strongly mylonitic syenite with variable amount and size of Kfs porphyroclasts (Fig. 6b) whose asymmetric recrystallization tails are formed exclusively of Kfs. The porphyroclasts show the same compositional range as the ones from undeformed samples (Fig. 5a). Undulose extinction is common, as well as 0.1–0.5 mm diameter subgrains which evolve to new grains at porphyroclast margins and tails (Fig. 8a and b). Exsolved albite commonly forms a thin film placed along subgrain boundaries or between recrystallized Kfs grains (arrows in Fig. 8b). The progression of Kfs porphyroclast recrystallization into granoblastic grains leads to the formation of lenslike granoblastic aggregates which alternate along the foliation with mafic aggregates to produce a discontinuous banding.

Clinopyroxene grain size ranges from 0.5 to 2 mm, and the larger ones behave like porphyroclasts in the groundmass (Fig. 8c). The average composition is very similar to the one obtained in the undeformed rock, $Wo_{44.5}En_{37.5}Fs_{17.1}Aeg_{0.75}$, and therefore slightly more magnesian than the primary ones (Fig. 5b). Cpx from DHSZ has locally developed recrystallized tails (Fig. 8c inset), with recrystallized grain size of about 0.1 mm and polygonal granoblastic texture. The recrystallized Cpx also have the same composition of the parent grain. Cpx recrystallization points to the high temperature and low water content of the system during the deformation in dry zones.

Biotite from the dry zone is optically similar to the primary one as far as grainsize, inclusions and absorption colour are concerned, but has slight compositional differences. Its Fe/(Fe + Mg) ratio is slightly lower than that of biotite from the undeformed zone (Fig. 5c), with values between 0.37 and 0.41, whilst $Al^{iv + vi}$ is slightly higher, ranging from *ca.* 2.3 to 2.5 a.f.u. Ti contents are also comparable to those of primary biotites, from 0.32 to 0.53 a.f.u. Cl contents, on the other hand, are up to eight times lower than that of the primary crystals, with values from 0.010 to 0.024 a.f.u. (Fig. 5d).

5.2.3. Microstructures and mineral composition of WHSZ

The typical feature of WHSZ is the mesoscale repetition of porphyroclastic syenite and quartz-plagioclase-rich ultramylonites. In the porphyroclastic syenite, discontinuous banding is characterized by interspersed biotite-rich layers and very elongate, quartz-feldsphatic lenses which surround porphyroclast systems, the latter being the main strain marker in the mylonitic rocks (Fig. 9). Their asymmetric tails and the angle between their long axes and the foliation indicate dextral shearing.

5.2.3.1. K-feldspar porphyroclasts and intergrowth mantles. A porphyroclast system consists of a relict core of perthitic Kfs, and an intergrowth mantle of variable thickness which may be continuous into an asymmetric recrystallization tail. Within the mantle, myrmekite replaces Kfs preferentially along planes facing the foliation, and coarse (up to 5 mm) plagioclase + quartz, micrographic intergrowths may crystallize in strain shadows (Fig. 10a and b). Kfs ranges in composition from Or_{88} Ab_{12} to Or_{96} Ab_{04}, whilst plagioclase from the mantle falls in two compositional

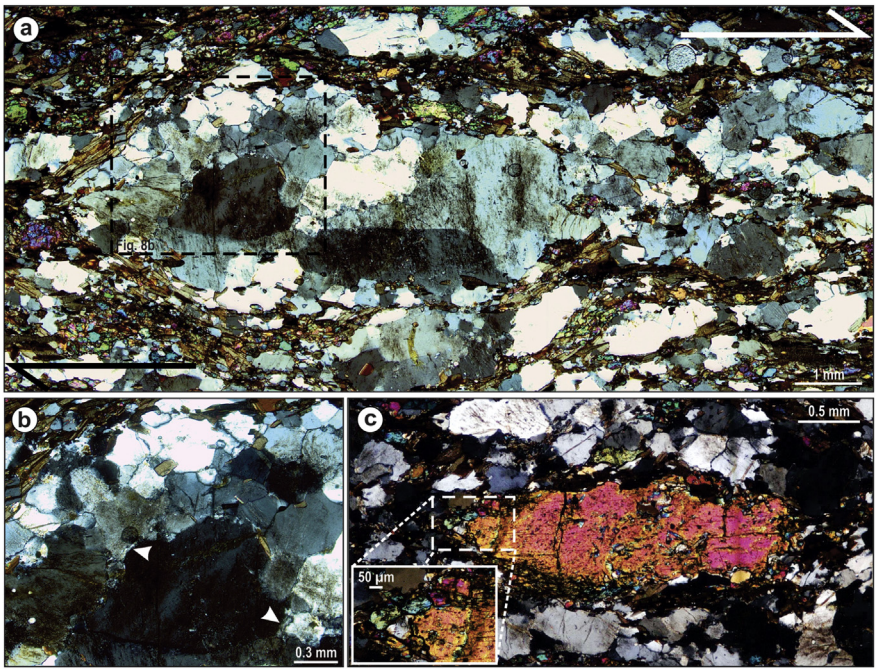

Fig. 8. Microstructural features of APS in dry high-strain zones. (a) Dextral Kfs porphyroclast with large subgrains and recrystallized grains. Notice the relatively large size of recrystallized grains. (b) Enlargement of area indicated by dashed line in (a) to show triple junctions between recrystallized grains. White arrows indicate the exsolution of perthite preferentially along the boundary between porphyroclast core, and recrystallized mantle. (c) Cpx porphyroclast with fine recrystallized grains at the tip (enlarged in the inset).

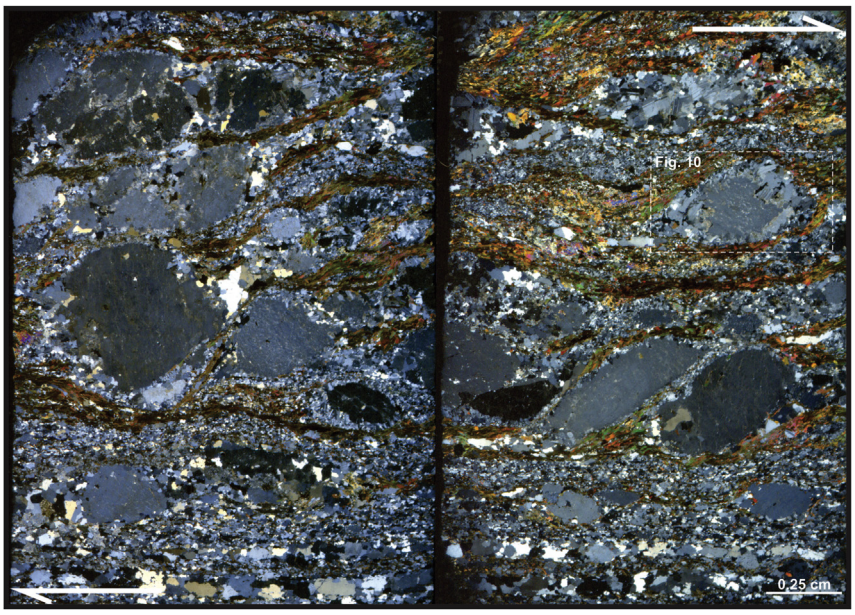

Fig. 9. Microstructural features of APS in wet high-strain zones. In the lower part of the photograph (corresponding to the bracket in Fig. 6c) (quartz + plagioclase)-rich, mylonitic groundmass is dominant, whilst the upper part features different stages of myrmekite rim development around asymmetric porphyroclasts of dextral shear sense surrounded by the mylonitic foliation and mm-thick banding. Dashed rectangle indicates zoom area in Fig. 10.

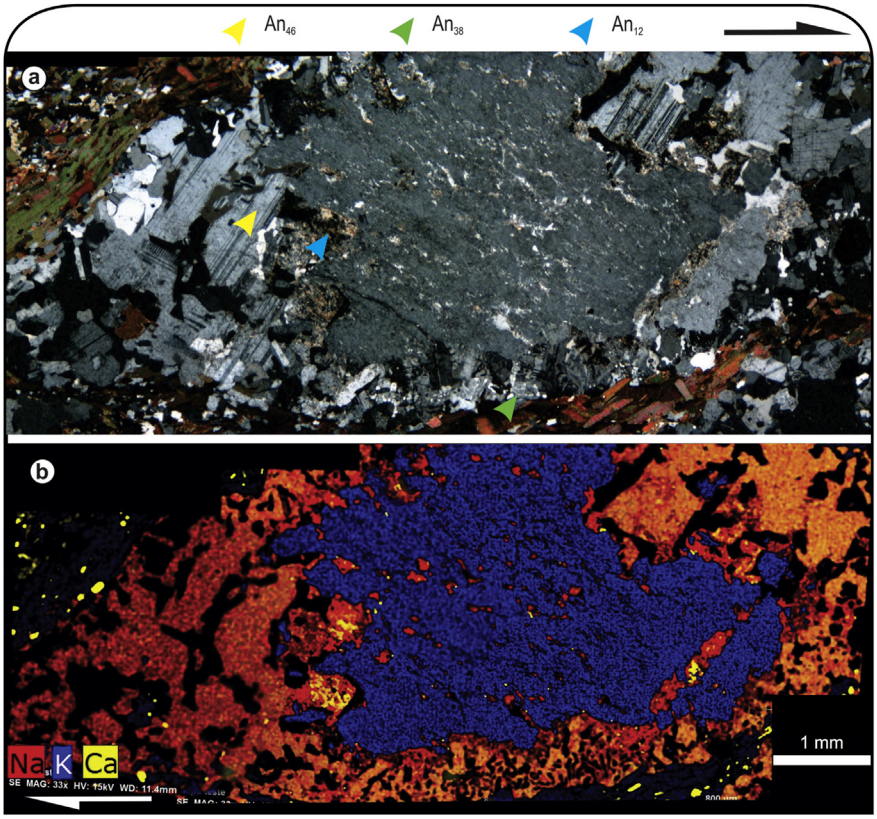

Fig. 10. Photomicrograph (a) and SEM compositional map (b) of a Kfs porphyroclast (area indicated in Fig. 9) partially substituted by foliation-parallel myrmekite mantle and micrographic coarse-grained aggregate of plagioclase and quartz crystallized in strain shadows. Black patches within orange areas in (b) are myrmekite, wormlike quartz grains in the central bottom part, and irregular coherent intergrowths within plagioclase of left and right strain shadows. Arrow colours in (a) indicate different plagioclase compositions obtained by microprobe analysis. Notice indented contact between porphyroclast core and mantle.

groups of andesine (Fig. 5a). Myrmekitic plagioclase is An_{38-41} (green arrow in Fig. 10a). In micrographic intergrowths it ranges from An_{42} to An_{48} (yellow arrow in Fig. 10a). Kfs cores are 1–20 mm in diameter and show virtually no intracrystalline

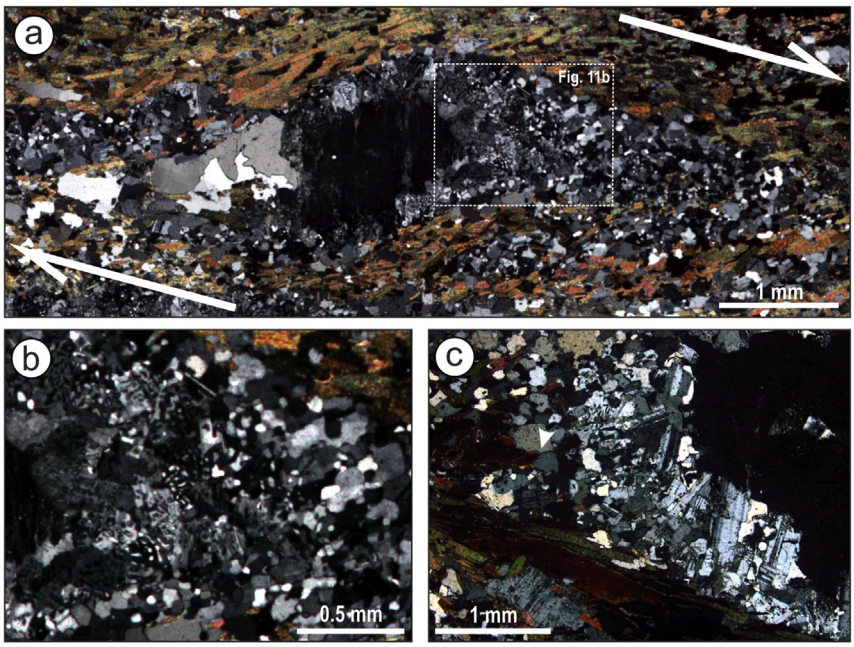

Fig. 11. Microstructural features from the wet zone mylonites. (a) Well-developed myrmekite mantle around Kfs porphyroclast, with dextral shear sense indicated by recrystallized tail asymmetry. Progression from myrmekite mantle to recrystallized tail is indicated by dashed rectangle and shown in detail (b). (c) Large euhedral plagioclase grains formed at the margin of Kfs core.

deformation. Therefore, undulose extinction or subgrains are only local and poorly developed in these relict cores. Fractures parallel to cleavage planes are occasionally filled by quartz, secondary minerals and, more rarely, fine myrmekite. The irregular yellow patches within the reddish orange area near the Kfs core of Fig. 10b is due to Ca-rich white-micas, and the nearby plagioclase composition is albitic (An_{9-12} – blue arrow in Fig. 10a). Additionally, these minerals may form along the Kfs cleavages (right-hand side of Fig. 10). Such features are interpreted to result from the late-hydrothermal alteration of andesine.

Myrmekites nucleate preferentially along foliation-parallel faces, but may progressively develop into a full, usually thicker (up to 1.5 mm) rim, as shown in Fig. 11. Plagioclase from the myrmekite mantles is *ca.* 0.5 mm in size. Contacts between core and mantle are usually sinuous, as shown in the enlargement of Fig. 11b. The rim material may locally grow into the core along cleavage planes and other discontinuities, which suggests a percolative character of the replacement process. A gradation from myrmekite to a very fine-grained polygonal granoblastic texture is observed from the inner to the outer part of the rim, the incomplete process leading to coexistence of individual quartz blebs and granoblastic grains within the porphyroclast tail (Fig. 11b).

The large plagioclase grains from the strain shadows are anhedral and exhibit sutured contacts with the Kfs core. They form coherent intergrowths with irregular quartz grains that tend to grow alternately along different twin boundaries of the plagioclase (Fig. 10), and are thus considered as a type of micrographic intergrowth. These micrographic intergrowths are also progressively recrystallized into the clast tails. An additional textural type of plagioclase found in the mantles is represented by subhedral grains (ca. 1 mm) whose An content is similar to the ones found in micrographic aggregates (Fig. 11c).

The progressive replacement of Kfs by quartz + plagioclase intergrowths and their recrystallization, as described above, sometimes leads to nearly complete substitution of the porphyroclasts by (quartz + plagioclase)-rich lenses of granoblastic aggregates

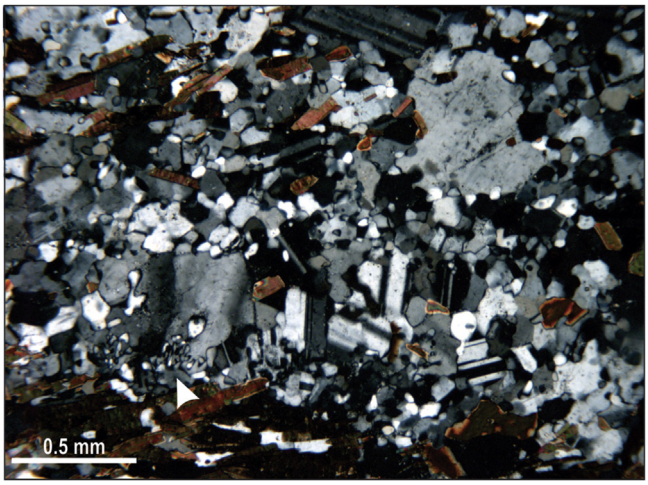

Fig. 12. Myrmekite relict (white arrow) in the very fine-grained (plagioclase + quartz)-rich mylonitic rock.

(Fig. 12) which contribute to the observed mm-thick banding of the rock in thin section (Fig. 9). These may also form thicker bands (lower part of Fig. 9), and eventually outcrop-scale bands (Fig. 6a).

5.2.3.2. Biotite texture and composition of the WHSZ relative to that of other structural domains. Biotite is the main mafic phase in the WHSZ and occurs in two generations, recognized initially by their texture. The primary-looking ones are dominant, with grain size, absorption colour and inclusions similar to the ones found in the undeformed and DHSZ counterparts. Their composition, as compared to the biotite from the other domains shows higher contents of Al^t (2.40–2.50) (Fig. 5c) with intermediate values of Fe/(Fe + Mg) (0.38–0.42) and Cl (0.022–0.395) (Fig. 5d). The Ti

content is compatible with those of undeformed and dry zone samples (0.28–0.44 a.f.u.).

The second generation of biotite is finer-grained (0.05–0.1 mm) and occurs either at the tips of strain shadows or as very fine trails in the recrystallized mantle, branching from biotite-rich layers. It is in textural equilibrium with recrystallized quartz and plagioclase grains (arrow in Fig. 11c). The composition of this finer biotite is similar to that of the coarser ones (Fig. 5c and d).

The two generations of biotite from the WHSZ and biotites from the DHSZ have parallel negative trends for Fe/(Fe + Mg) and Al^t. They are both distinguished from biotites from the undeformed syenite by their lower Fe/(Fe + Mg) and higher Al^t content, especially those from the WHSZ (Fig. 5c). The Cl content is the best discrimination parameter of biotites from different structural domains (Fig. 5d). It is highest in the undeformed rocks, with intermediate values in the WHSZ biotites and lowest in the DHSZ. A general positive trend of Cl with Fe/(Fe + Mg) contents is also apparent in this diagram.

6. Model for strain partitioning into dry and wet high-strain zones

In order to illustrate the proposed model, Fig. 13 shows the evolution stages in the strain partitioning of the studied syenites. Magmatic structures have been developed by flow during syntectonic emplacement (Fig. 13a). Continuous, heterogeneous deformation has promoted progressive development of mylonitic structures parallel to the primary ones during late-stage magmatic crystallization of the syenite. At the same stage (Fig. 13b) the increased water activity combined with heterogeneous strain-enhanced transport (Tullis et al., 1996; Brown and Solar, 1998) of the residual magma through pre-existing foliations in high-strain zones was responsible for de-stabilization and resorption of early-formed igneous Cpx. Cpx dissolution released Ca^{++} to the magmatic liquid, and minor amounts of Cpx could have been replaced by amphibole, which would also release Ca^{++}. Kfs in turn, as the largest size active marker in the syenite, has promoted liquid concentration in surrounding dilatant sites and then became unstable under Ca-enriched conditions, being replaced by andesine plus quartz (Fig. 13c – upper inset). Contrasting texture and microstructure, as well as slightly different composition of the newly-formed plagioclase suggest two different kinds of interaction between the early-crystallized Kfs and the Ca-enriched, late-magmatic liquid: (i) Coupled dissolution of Kfs and magmatic crystallization of undeformed, calcium-rich plagioclase (An_{42-48}) which forms either anhedral grains in micrographic intergrowths with quartz, or finer prismatic grains; (ii) Direct replacement of Kfs by myrmekite with slightly more sodic plagioclase (An_{38-41}). The more sodic composition of this plagioclase is probably due to a greater contribution of the perthitic component in the replacement of Kfs. Mineral crystallization in dilatant sites was probably accompanied by coupled partial dissolution of the Kfs porphyroclast, since their core-mantle boundary is invariably sutured (Fig. 10). The K^+ ions expected to have been released during partial dissolution or replacement of Kfs could have been used to form second-generation biotite. A qualitative bulk reaction matching Cpx dissolution/hydration and Kfs dissolution-replacement by myrmekite may be written as follows:

$$\text{Kfs} + \text{Cpx} + \text{water-rich magmatic liquid} = \text{Ad} + \text{Qtz} + \text{Bt} (\pm\text{Am})$$

The presence of micrographic intergrowth in strain shadows is indicative of the water-rich condition of the late-magmatic liquid (Fenn, 1986) necessary to start Cpx dissolution. On the other hand, the occurrence of myrmekites unrestricted to porphyroclast faces parallel to the main foliation, in some cases forming complete rims (Fig. 11), points to the increasing importance of liquid infiltration, instead of stress concentration, as the main control of the reaction sites during progressive deformation. This is also in agreement with previous data, as in Menegon et al. (2006). Accordingly, the Cl content of biotite in WHSZ is approximately twice that observed in DHSZ biotite. These values confirm the more significant role played by fluids in the WHSZ when compared with the DHSZ, which is also in agreement with the comparison of the sum of hydrated phases (31.1 and 21.3%, respectively). The remaining late-magmatic fluids could have been responsible for the local hydrothermal alteration of andesine to albite plus Ca-rich white mica.

With progressive strain both types of substitution rims were further stretched and recrystallized. The reworking of the mantles would probably demand less energy than the recrystallization of the original Kfs megacrysts due to their initial polycrystalline character and to their previously reduced grain size. In these fine-grained domains, diffusion-accommodated grain-boundary sliding (Passchier and Trouw, 2005) was probably an additional deformation mechanism.

Progressive deformation of the intergrowth mantle has effectively contributed to the genesis of the mylonitic foliation (as argued by Vernon, 1991, Fig. 13c), and together with a predicted volume reduction caused by the myrmekite-forming reaction (as demonstrated by Simpson and Wintsch, 1989; Menegon et al., 2006) has favoured the continuous inflow of water-rich late-magmatic liquid. This has established a positive feedback between late-magmatic liquid inflow and strain/reaction softening in the wet zones, and promoted, in some cases, the complete replacement of Kfs. The end-member of this transformation in the APS was the generation of mm-to cm-thick bands of quartz-bearing ultramylonites of granodioritic modal composition where Kfs and myrmekite relicts are set in a very fine-grained granoblastic groundmass composed mainly of plagioclase plus quartz (Fig. 12), alternating with biotite-rich bands of approximately the same thickness (Fig. 9).

The DHSZ, on the other hand, represents areas neighbouring WHSZ which were drained (or maintained dry) and became melt-poor. The primary mineralogy was preserved and the deformation mechanisms were not influenced by the presence of melt in disequilibrium, but instead were controlled by the granulite-facies conditions (Fig. 13c – lower inset). Kfs was recrystallized probably by subgrain rotation recrystallization (Passchier and Trouw, 2005). Clinopyroxene was also recrystallized, although to a lesser extent. The composition of DHSZ Cpx porphyroclasts and recrystallization tails are virtually the same as in the undeformed syenite. Such result points toward compatible conditions of crystallization and recrystallization of the system, which is another piece of evidence for the syntectonic character of the APS.

Apart from the differences between wet and dry high-strain zones, the consistency of shear-sense indicators and the multiple lines of evidence of syntectonic character of the magmatism indicates synchronous or progressive development of high-T deformation/crystallization in these different domains, thus indicating strain partitioning, with fluid-enhanced, highest strain concentration in the WHSZ.

In summary, both dissolution of Cpx and replacement of Kfs (directly by myrmekite-forming reaction or by coupled dissolution and crystallization of andesine plus quartz from the late-magmatic liquid) have acted together through melt-assisted dissolution-replacement creep to transform the mineral composition of APS in the WHSZ. This caused strain softening and a positive feedback

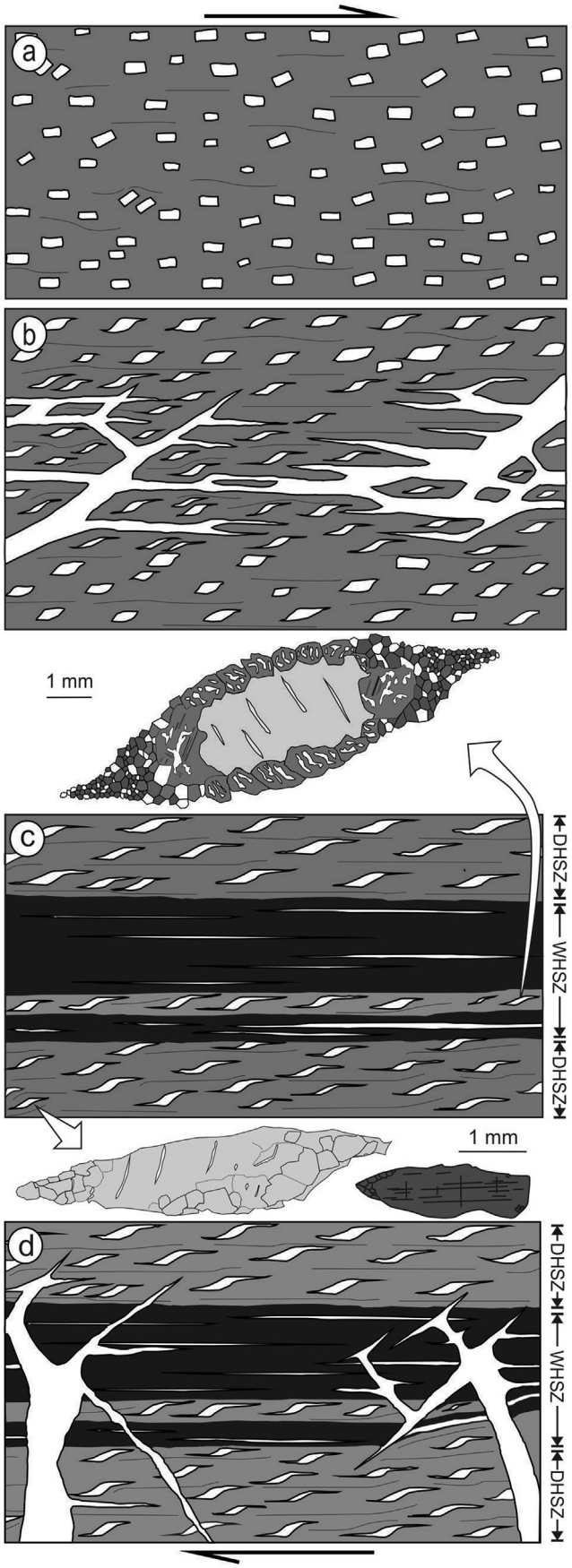

with continuous water-rich magma inflow, whilst the adjacent rock volume was deformed under dry conditions and the mineralogy remained essentially stable (Fig. 13d).

7. Final remarks

The compatibility of deformation between dry and wet high-strain zones of the APS is expressed by the concordance of structures and consistency of shear-sense indicators. Strain partitioning into dry and wet high-strain zones, and the fact that widespread myrmekite is restricted to the latter, demonstrates that in this case fluids are the necessary triggering factor to promote the formation of myrmekites.

In the APS, more than one variable has contributed to allow melt-assisted dissolution-replacement creep to operate in the WHSZ. Among them, we highlight the high temperature of granulite facies environment and the fertile composition of the ultrapotassic syenitic system which have acted together to permit the development of the observed features.

The high temperature of the system must have been kept near the solidus for a time-span long enough to permit: i) the strain-assisted transport of the water-rich, late-magmatic liquid throughout high-strain zones; and ii) the re-equilibration of the early-crystallized phases (Kfs and Cpx) by dissolution and replacement in the presence of this liquid.

On the other hand, the fertile composition of the ultrapotassic syenite determined the nature of these re-equilibrium reactions. They are essentially due to the existence of an early crystallized anhydrous Ca-rich phase (Cpx) and to the Ca-poor main mineral (Kfs). Both phases became unstable due to the percolation of water-rich, late-magmatic liquid and the consequent increase of Ca^{++} released from the first. The Ca-rich composition of plagioclase from the studied myrmekites results from the Ca-rich nature of the percolating liquid, which in turn results from the destabilization of Cpx. The ultimate progression of this transformation process has locally produced granodioritic modal compositions from syenitic magmas by interaction of early-crystallized phases and water-rich, late-magmatic liquids under high-strain, high-T conditions.

Myrmekite genesis is accompanied by drastic grain size reduction and volume decrease, thus enhancing plastic behaviour and permeability, which in turn assists fluid inflow. Pervasive myrmekite formation as a consequence of deformation coupled with late-magmatic liquid flow in syntectonic environments may contribute significantly to deformation partitioning and strain softening in the

Fig. 13. - Cartoon depicting successive stages in the model proposed for strain partitioning into dry and wet high strain zones of the studied syenites. (a) Development of magmatic foliation marked by shape orientation of both K-feldspar phenocrysts and matrix material; (b) progressive deformation of the mush is accompanied by heterogeneous injection of fluid-rich late-magmatic liquids, which facilitates strain softening; (c) the positive feedback between deformation and fluid-rich magma inflow leads to strain partitioning into dry high strain zones (DHSZ) and wet high strain zones (WHSZ). Microstructures of the WHSZ (upper inset) points to melt-assisted dissolution-replacement creep mechanisms: dissolution of clinopyroxene (no longer found in these rocks) by fluid-rich late-magmatic liquids release Ca^{++} to replacement reactions of K-feldspar by myrmekite (plagioclase An_{38-41}) and coupled dissolution of K-feldspar and igneous crystallization of micrographic intergrowth and subhedral plagioclase (An_{42-48}). These intergrowths are reworked by dynamic recrystallization due to strain softening. DHSZ microstructures (lower inset) result from dislocation creep mechanisms with K-feldspar recrystallization by progressive rotation of subgrains and local recrystallization of clinopyroxene. (d) WHSZ are continuously re-injected. Early injections are disrupted and enhance ultramylonite banding. Younger, less deformed injections crosscut early-formed ones. DHSZ remain so because they are not injected by late-magmatic liquids. Original mineralogy is preserved, despite high strain concentration. In order to best illustrate overall aspects, figures a-d are out of scale.

lower continental crust, thus expanding the field where dissolution-replacement creep operates. The proposed model may be able to account for significant changes in the lower-crust rheology.

Acknowledgements

We thank the Brazilian National Research Council (CNPq) for the MSc (G.B. De Toni) and Productivity grants (M.F. Bitencourt and L. Nardi). G.B. De Toni is grateful to Samuel Sbaraini, Evelin Schnorr, Pedro Andrade and Amós Martini for their help with field work and graphic editing. The text was greatly improved after discussions and reviews by Luiz F.G. Morales, Roberto Weinberg, Luca Menegon and Kyuichi Kanagawa.

Appendix A. Supplementary data

Supplementary data related to this article can be found at http://dx.doi.org/10.1016/j.jsg.2016.08.002.

References

Abart, R., Heuser, D., Habler, G., 2014. Mechanisms of myrmekite formation: case study from the Weinsberg granite, Moldanubian zone, Upper Austria. Contrib. Mineral. Petrol. 168 (5), 1–15.
Almeida, F.F.M., de Brito Neves, B.B., Carneiro, C.D.R., 2000. The origin and evolution of south american platform. Earth-Sci. Rev. 50, 77–111.
Álvares-Valero, A.M., Cesare, B., Kriegsman, L.M., 2005. Formation of elliptical garnet in a metapelitic enclave by melt-assisted dissolution and reprecipitation. J. Metamorph. Geol. 23, 65–74.
Ashworth, J.R., 1972. Myrmekites of exsolution and replacement origins. Geol. Mag. 109, 45–62.
Becke, F., 1908. Ueber myrmekite. Schweiz. Mineral. Petrogr. Mittl. 27, 377–390.
Bitencourt, M.F., Nardi, L.V.S., 2000. Tectonic setting and sources of magmatism related to the southern Brazilian shear Belt. Braz. J. Geol. 30, 186–189.
Bitencourt, M.F., De Toni, G.B., Florisbal, L.M., Martil, M.M.D., Niessing, M., Gregory, T.R., Nardi, L.V.S., Heaman, L.M., Dufrane, S.A., 2011. Structural geology and U-Pb age of unusual Neoproterozoic syn-collisional syenite-tonalite association from southernmost Brazil. In: Seventh Hutton Symposium on Granites and Related Rocks, Abstracts Book. Universidad de Salamanca, Avila, 21.
Bitencourt, M.F., Nardi, L.V.S., De Toni, G.B., Florisbal, L.M., 2013. Neoproterozoic late to post-collisional, quartz-bearing ultrapotassic syenites from southernmost Brazil. In: Goldschmidt2013, Conference Abstracts, Florence, 710. http://dx.doi.org/10.1180/minmag.2013.077.5.2.
Bitencourt, M.F., Nardi, L.V.S., Florisbal, L.M., Heaman, L.M., 2015. Geology, geochronology and petrogenesis of a Neoproterozoic, syntectonic sillimanite-muscovite-biotite granite from southernmost Brazil. In: The 8th Hutton Symposium on Granites and Related Rocks, Book of Abstracts.
Brown, M., Solar, G.S., 1998. Shear-zone systems and melts: feedback relations and self-organization in orogenic belts. J. Struct. Geol. 20, 211–227.
Chemale Jr., F., Philipp, R.P., Dussin, I.A., Formoso, M.L.L., Kawashita, K., Berttotti, A.L., 2011. Lu–Hf and U–Pb age determination of Capivarita anorthosite in the Dom Feliciano Belt, Brazil. Precambrian Res. 186, 117–126.
Deer, W.A., Howie, R.A., Zussman, J., 1992. An Introduction to the Rock-forming Minerals, seco[nd] ed. In: Longman Scientific & Technical. Wiley, Harlow, Essex; New York.
Dymek, R.F., Schiffries, C.M., 1987. Calcic myrmekite: possible evidence for the involvment of water during the evoltion of andesine anorthosite from St-Urbain, Quebec. Can. Mineral. 25, 291–319.
Efimov, A.A., Flerova, K.V., Maegov, V.I., 2010. The first find of calcic myrmekite (Quartz-plagioclase symplectites) in Uralian Gabbro. Dokl. Earth Sci. 435, 1450–1455.
Etheridge, M.A., Wall, V.J., Vernon, R.H., 1983. The role of fluid phase during regional metamorphism and deformation. J. Metamorph. Geol. 1, 205–226.
Fenn, P.M., 1986. On the origin of graphic granite. Am. Mineralogist 71, 325–330.
Fernandes, L.A.D., Tommasi, A., Porcher, C.C., 1992. Deformation patterns in the southern Brazilian branch of the Dom Feliciano Belt: a reappraisal. J. S. Am. Earth Sci. 5, 77–96.
Hartmann, L.A., Santos, J.O.S., Philipp, R.P., McNaughton, N.J., 2011. Time frame of 753-680 Ma juvenile accretion during São Gabriel orogeny, southern Brazil. Gondwana Res. 19, 84–99.
Kretz, R., 1983. Symbols for rock-forming minerals. Am. Mineralogist 68, 277–279.
Kruhl, J.H., 1996. Prism- and basal-plane parallel subgrain boundaries in quartz: a microstructural geothermobarometer. J. Metamorph. Geol. 14, 581–589.
Mainprice, D., Bouchez, J.L., Blumenfeld, P., Tubia, J.M., 1986. Dominant *c* slip in naturally deformed quartz: implications for dramatic plastic softening at high temperature. Geology 14, 819–822.
Martil, M.M.D., Bitencourt, M.F., Nardi, L.V.S., 2011. Caracterização estrutural e petrológica do magmatismo pré-colisional do Escudo Sul-rio-grandense: os ortognaisses do Complexo Metamórfico Várzea do Capivarita. Pesqui. em Geociências 38, 181–201.
Martil, M.M.D., Bitencourt, M.F., Armstrong, R., Nardi, L.V.S., Chemale Jr., F. Geochronology of Orthogneisses from the Várzea Do Capivarita Complex Thrust Pile and Implications for the Timing of Continental Collision in Southernmost Brazil. Precambrian Research, (under review).
Menegon, L., Pennacchioni, G., Stünitz, H., 2006. Nucleation and growth of myrmekite during ductile shear deformation in metagranites. J. Metamorph. Geol. 24, 553–568.
Menegon, L., Pennacchioni, G., Spiess, R., 2008. Dissolution-precipitation creep of K-feldspar in mid-crustal mylonites. J. Struct. Geol. 30, 565–579.
Morimoto, N., 1988. Nomenclature of pyroxenes. Mineral. Mag. 52, 535–550.
Mukai, H., Austrheim, H., Putnis, C.V., Putnis, A., 2014. Textural evolution of plagioclase feldspar across a shear zone: implications for deformation mechanism and rock strength. J. Petrol. 55, 1457–1477.
Niessing, M., Bitencourt, M.F., Kruhl, J.H., Vlach, S.R.F., 2011. Sillimanite-bearing, S-type granite from post-collisional environment in southern Brazil. In: Seventh Hutton Symposium on Granites and Related Rocks, Avila, Spain, July 4-9 2011. Abstracts Book. Universidad de Salamanca, Avila, p. 109.
Parsons, I., Brown, W.L., 1983. A TEM and microprobe study of a two-perthite alkali Gabbro: implications for the ternary feldspar system. Contrib. Mineral. Petrol. 82, 1–12.
Passchier, C.W., Trouw, R.A.J., 2005. Microtectonics, seco[nd] ed. Springer-Verlag, Heidelberg.
Philipp, R.P., Machado, R., 2005. The late Neoproterozoic granitoid magmatism of the Pelotas Batolith, southern Brazil. J. S. Am. Earth Sci. 19, 461–478.
Philipp, R.P., Machado, R., Nardi, L.V.S., Lafon, J.M., 2002. O Magmatismo Granítico Neoproterozóico do Batólito Pelotas no sul do Brasil: Novos dados e revisão da Geocronologia regional. Braz. J. Geol. 32, 277–290.
Philipp, R.P., Bom, F.M., Pimentel, M.M., Junges, S.G., Zvirtes, G., 2015. SHRIMP U-Pb age and high temperature conditions of the collisional metamorphism in the Várzea do Capivarita Complex: implications for the origin of Pelotas Batholith, Dom Feliciano Belt, southern Brazil. J. S. Am. Earth Sci. 66, 196–207.
Phillips, E.R., 1974. Myrmekite – one hundred years later. Lithos 7, 181–194.
Phillips, E.R., 1980. On polygenetic myrmekite. Geol. Mag. 117, 29–36.
Schwantke, A., 1909. Die beimischung von Ca in Kalifeldspat und die Myrmekitbildung. Zentralblatt für Geol. Palaontologie 311–316.
Simpson, C., Wintsch, R.P., 1989. Evidence for deformation-induced K-feldspar replacement by myrmekite. J. Metamorph. Geol. 7, 261–275.
Smith, J.V., Brown, W.L., 1988. Feldspar Minerals, seco[nd] ed., vol. 1. Springer-verlag, Heidelberg.
Tsurumi, J., Hosonuma, H., Kanagawa, K., 2003. Strain localization due to a positive feedback of deformation and myrmekite-forming reaction in granite and aplite mylonites along the Hatagawa Shear Zone of NE Japan. J. Struct. Geol. 25, 557–574.
Tullis, J., Yund, R., Farver, J., 1996. Deformation-enhanced fluid distribution in feldspar aggregates and implications for ductile shear zones. Geology 24, 63–66.
Vernon, R.H., 1991. Questions about myrmekite in deformed rocks. J. Struct. Geol. 13, 979–985.
Vernon, R.H., 2004. A Practical Guide to Rock Microstructure. Cambridge University Press, Cambridge.
Voll, G., 1960. New work on petrofabrics. Liverp. Manch. Geol. J. 2, 521–525.
Wintsch, R.P., Yi, K., 2002. Dissolution and replacement creep: a significant deformation mechanism in mid-crustal rocks. J. Struct. Geol. 24, 1179–1193.